# Small anticancer drug release by light: Photochemical internalization of porphyrin-$\beta$-cyclodextrin nanoparticles

Stylianos Panagiotakis, Barbara Mavroidi, Alexandros Athanasopoulos, Antonio Ricardo Gonçalves, Loïc Bugnicourt-Moreira, Theo Regagnon, Nikos Boukos, George Charalambidis, Athanasios Coutsolelos, Mantas Grigalavicius, et al.

# Small anticancer drug release by light: photochemical internalization of porphyrin-β-cyclodextrin nanoparticles

Stylianos Panagiotakis,[a] Barbara Mavroidi,[b] Alexandros Athanasopoulos,[b] Antonio Ricardo Gonçalves,[a] Loïc Bugnicourt-Moreira,[c] Theo Regagnon,[c] Nikos Boukos,[a] George Charalambidis,[d] Athanasios G. Coutsolelos,[d] Mantas Grigalavicius,[e] Theodossis A. Theodossiou,[e] Kristian Berg,[e] Catherine Ladavière,[c] Maria Pelecanou,[b] Konstantina Yannakopoulou*[a]

[a] Institute of Nanoscience and Nanotechnology, National Center for Scientific Research "Demokritos", Aghia Paraskevi 15341, Attiki, Greece

[b] Institute of Biosciences & Applications, National Center for Scientific Research "Demokritos", Aghia Paraskevi 15341, Attiki, Greece

[c] University of Lyon, CNRS, UMR 5223, IMP, UCBL, 15 bd André Latarjet, F-69622 Villeurbanne, France

[d] Laboratory of Bioinorganic Chemistry, Department of Chemistry, University of Crete, Voutes Campus, 70013 Heraklion, Crete, Greece

[e] Department of Radiation Biology, Institute for Cancer Research, Oslo University Hospital - Radium Hospital, 0379 Oslo, Norway

Stylianos PANAGIOTAKIS: s.panagiotakis@inn.demokritos.gr
Barbara MAVROIDI: bmavroidi@bio.demokritos.gr
Alexandros ATHANASOPOULOS: alexandr@bio.demokritos.gr
Loïc BUGNICOURT-MOREIRA: loic.bugnicourt@hotmail.com
Théo REGAGNON: tregagnon@hotmail.fr
Antonio Ricardo GONÇALVES: aricardo7@gmail.com
Nikos BOUKOS, n.boukos@inn.demokritos.gr
Georgios CHARALAMBIDIS: gcharal@uoc.gr
Athanassios G. COUTSOLELOS: acoutsol@uoc.gr
Mantas GRIGALAVICIUS: mangri@rr-research.no
Theodossis A. THEODOSSIOU: Theodossis.Theodossiou@rr-research.no
Kristian BERG: Kristian.Berg@rr-research.no
Catherine LADAVIERE: Catherine.Ladaviere@univ-lyon1.fr
Maria PELECANOU: pelmar@bio.demokritos.gr

Corresponding author: Konstantina YANNAKOPOULOU: k.yannakopoulou@inn.demokritos.gr, Tel. +30-210-6503796, Fax : +30-210-651766. ORCID iD 0000-0002-0725-4906

**Highlights**

- New, neutral, amphiphilic βCD-triphenylporphyrin conjugates were synthesized
- Although different, they all form very similarly sized nanoparticles (NPs)
- The NPs specifically target and accumulate in the lysosomes of MCF-7 cells
- The non-toxic NPs transport differently structured anticancer drugs to lysosomes
- Red light irradiation causes drug release conferring major and lasting toxicity to cells

## Abstract

Aiming to engineer simple, neutral, strongly amphiphilic photoactive nanoparticles (NPs) to specifically target cancer cell lysosomes for drug transport and light-controlled release, new conjugates of β-cyclodextrin with highly hydrophobic triphenylporphyrin bearing different alkyl chains, were synthesized. Although differently sized, all conjugates self-assemble into ~60 nm NPs in water and display similar photoactivity. The NPs target selectively the lysosomes of breast adenocarcinoma MCF-7 cells, embedding in vesicular membranes, as experiments with model liposomes indicate. Either empty or drug-loaded, the NPs lack dark toxicity for 48 h. They bind with differently structured anticancer drugs tamoxifen and gemcitabine as its *N*-adamantyl derivative. Red light irradiation of cells incubated with drug-loaded NPs results in major reduction of viability (>85%) for 48 h displaying significant synergy of photo-chemotoxicity, as opposed to empty NPs, and to loaded non-irradiated NPs, in manifestation of photochemical internalization (PCI). Our approach expands the field of PCI into different small molecule chemotherapeutics.

*Keywords*: cyclodextrin-porphyrin conjugates, drug delivery, photochemical internalization.

## 1. Introduction

Carbohydrate-based drug delivery systems that upon light stimulation combine phototoxic and chemotoxic action in high synergy for tumor treatment are continuously sought (Zhang et al., 2022). Biocompatible, water soluble carrier systems can combine selectively and synergistically anticancer drugs with suitable photosensitizer (PS) molecules that upon illumination can induce formation of reactive oxygen species (ROS) that are deleterious to biological matter. The ideal combination would also be capable of targeting cell organelles as this is critical to achieve high complementary efficacy in inducing cancer cell death (Kessel et al., 2022). Photodynamic therapy (PDT), a modality relying on the preferential retention of PSs in solid tumor tissue, utilizes focused light, e.g. diode lasers, to initiate a photokilling process that spares healthy cells (Dolmans et al., 2003; Agostinis et al., 2011). Amongst the PSs used, porphyrins hold a prominent position, due to both favorable photophysical characteristics and relative molecular stability, compared to chlorins and bacteriochlorins (Dabrowski et al., 2016). However, their very low aqueous solubility and concomitant loss of photoactivity due to aggregation is a major obstacle for bio-applications, but this is a manageable issue for photochemical internalization (PCI), an advanced intervention that relies on endocytosis and requires that the drug is entrapped exclusively into endocytic vesicles (endosomes, lysosomes) while the PS is anchored in their membranes. Irradiation using a sub-lethal PDT dose results in membrane rupturing and drug release leading to synergistic photo and chemo-toxicity of tumor cells (Jerjes et al., 2020). PCI has been implemented using chiefly macromolecular toxins that are unable to penetrate the plasma membrane and are thus internalized by endocytosis, co-administered with a suitable photosensitizer (Sultan et al., 2016). Consequently, examples using small molecule chemotherapeutics in PCI protocols are scarce.

Cyclodextrins (CDs) are cyclic carbohydrate oligomers that form inclusion complexes with hydrophobic drugs and solubilize them in water. Natural or specifically modified CDs are used extensively as excipients in drug formulations (Saokham et al, 2018). Simple porphyrin-CD covalent conjugates are attractive because they combine photoactivity with drug inclusion and ease of synthesis. Although several conjugates have appeared in the literature as (Mavridis & Yannakopoulou, 2020; Singh et al., 2015) including an example originating from this lab (Theodossiou et al., 2015; Fraix et al,

2013), the importance of prior nanoparticle (NP) formation and optimization has neither been properly recognized nor investigated in detail, to our knowledge,

We hypothesized that by connecting the highly photoactive hydrophobic 5,10,15,20-tetraphenylporphyrin (**TPP**) *via* linker alkyl chains of variable length to hydrophilic βCD we would create stable, small NPs by self-assembly in water. The hydrophobic linkers are expected to further modulate the amphiphilicity of the neutral conjugates, promote their molecular plasticity and capacity for self-assembly and augment their ability for encapsulation and transport of small anticancer drugs. If suitably sized, the photosensitive NPs will target endosomes/lysosomes of cells by endocytosis, carrying the bound drugs along. Apart from tamoxifen, an anticancer drug with multiple phenyl groups that match the βCD cavity size (Aggelidou et al., 2013), gemcitabine, although unsuitably structured, could also be effective if first converted into its *N*-adamantyl pro-drug. Both were expected to bind tightly enough to NPs to ensure co-delivery to lysosomes. The proposed approach would provide a widened choice of vehicles and small chemotherapeutics for the PCI technology.

Herein we use 2, 5 and 11-carbon chain linkers to connect **TPP** to βCD (Scheme 1) and demonstrate the successful formation of photoactive NPs that bind and transport the above mentioned small chemotherapeutics, specifically targeting the lysosomes of tumor cells. The NPs, devoid of dark toxicity, exert highly synergistic phototoxic and chemotoxic action upon illumination. Moreover, we employ photoactive liposomes as model vesicles in order to mimic organelles and understand the subcellular fate of our systems.

## 2. Results and Discussion

### *2.1. Synthesis and structural characterization*

Three porphyrin-βCD conjugates **TPPOCNHbmCx** (Scheme 1) were prepared by amide coupling between mono(6-amino-6-deoxy)-βCD (**bmNH$_2$**, Petter et al., 1990) and 5-(4-carboxyalkyloxy)phenyl]-10,15,20-triphenylporphyrins (**TPPOCOOHCx**, Panagiotakis et al., 2022) of variable alkyl chain length (2 to 11 C-atoms, Scheme A1). Reactions were successful only with 4-(4,6-dimethoxy-1,3,5-triazin-2-yl)-4-methylmorpholinium chloride (DMTMM, Kunishima et al., 1999), as trials with other coupling reagents lead to the recovery of the starting materials. The molecular structure

of the conjugates was confirmed with spectroscopic methods. FT-IR measurements of the solid conjugates do not support self-inclusion of **TPP** into βCD (Figs. A1-A15).

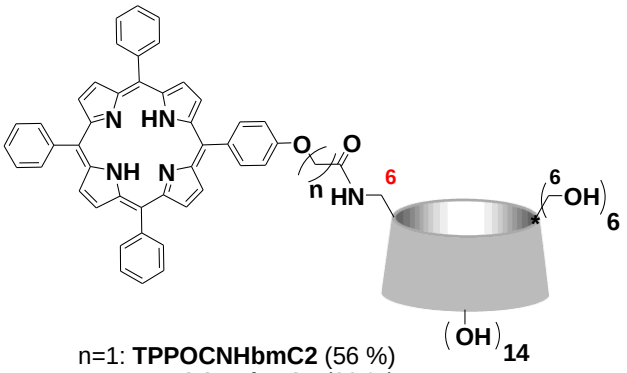


n=1: **TPPOCNHbmC2** (56 %)
n=4: **TPPOCNHbmC5** (82 %)
n=10: **TPPOCNHbmC11** (94 %)

**Scheme 1**. Molecular structure of the porphyrin-βCD conjugates, **TPPOCNHbmCx**, and % yields of their synthesis from porphyrins **TPPOCOOHCx** and mono(6-amino-6-deoxy)-βCD (**bmNH$_2$**).

*2. 2. Photophysical characterization*

*2.2.1. UV-Vis spectra in DMF and in aqueous solution:* The spectra of the conjugates and the corresponding parent porphyrins in the monomerizing (Shi & Linhardt, 2021) solvent DMF (Figs. 1A and 1B, respectively, Table B1) display characteristic absorption features (Panagiotakis et al., 2022; Mandal et al., 2016; Ormond & Freeman, 2013) with Soret (418.5 nm) and Q bands (500 - 675 nm). The Soret band intensities of **TPPOCNHbmC2** and **TPPOCNHbmC5** drop by ~75% and ~25%, respectively, relative to that of **TPPOCNHbmC11** (Fig. 1A) thus, the shorter the separation of the carbonyl group from the porphyrin $\pi$-system the higher the hypochromic effect observed. In phosphate buffer saline containing 4% DMSO (v/v), pH 7.4 (PBS) the spectra of the conjugates are not as severely affected, compared to their parent porphyrins while **TPPOCNHbmC11** displays remarkable recovery of its absorbance (Figs. 1C *vs* 1D). The Soret bands are relatively symmetrical with less pronounced "shoulders" on both sides of $\lambda_{max}$ and narrower at FWHM by ~ 4 - 38 nm, suggesting presence of rather uniform populations of species in PBS, compared to the parent porphyrins.

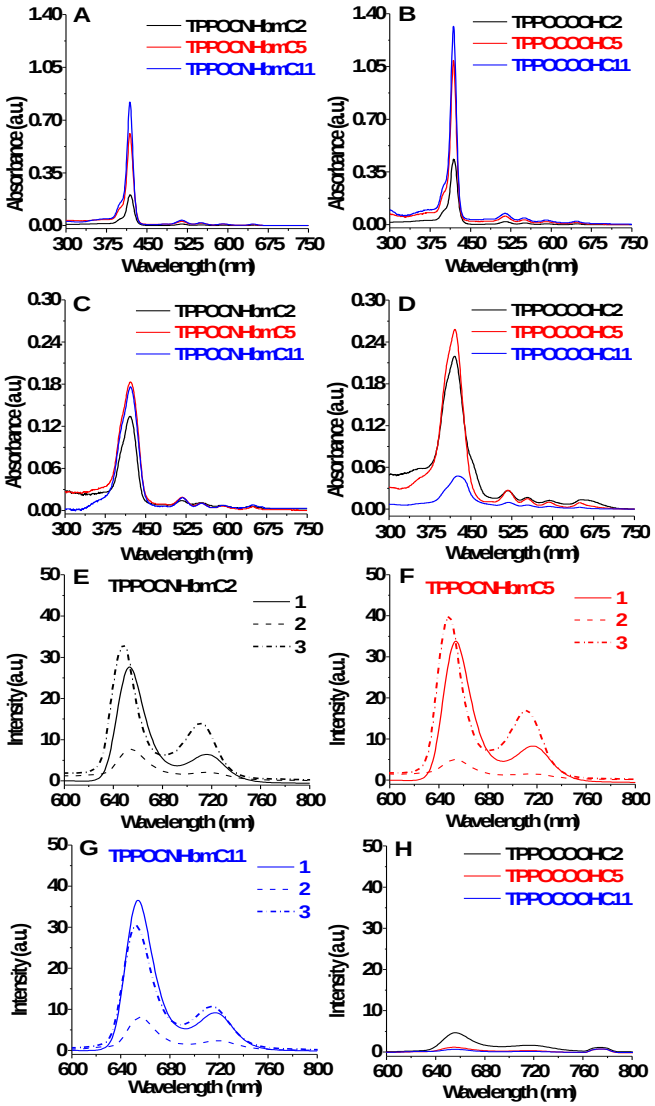


**Fig. 1.** UV-Vis absorption spectra (2 μM solutions): A) **TPPOCNHbmCx**, DMF; B) **TPPOCOOHCx**, DMF; C) **TPPOCNHbmCx,** PBS; D) **TPPOCOOHCx**, PBS. Emission spectra (2 μM solutions, A = 0.02, $\lambda_{exc}$ = 515 nm) of: E) **TPPOCNHbmC2**; F) **TPPOCNHbmC5**; G) **TPPOCNHbmC11** in **1**: (——) DMF; **2**: (- - -) PBS; **3**: (**.** - **.** - **.**) PBS with excess pMβCD (8 μM); H) **TPPOCOOHCx**, PBS (773 nm band arises from scattering of excitation light). The concentrations in DMF were adjusted to A = 0.02 at $\lambda_{exc}$ = 515 nm to enable comparison with the spectra in PBS.

*2.2.2. Emission spectra in DMF and in aqueous solution:* In DMF and $\lambda_{exc}$= 515 or 510 nm two characteristic emission bands at 653 and 717 nm are observed (Fig. 1E1,F1,G1, Fig. B15, Table B1). In PBS and $\lambda_{exc}$= 515 nm the intensities of these emission bands are significantly diminished (Fig. 1E2,F2,G2, Fig. B15C, Table B2), but still, two-, three- or ten-fold increased, compared to the parent **TPPOCOOHCx** (Fig. 1H). To assess the emission properties of the conjugates in

*monomeric* form in aqueous solution, we formed strong inclusion complexes *in situ* with 2,3,6-per-*O*-methyl-βCD (pMβCD), that specifically binds the **TPP** moiety (Table B3) as previously demonstrated with the parent porphyrins (Panagiotakis et al., 2022). Up to 3-fold enhancement of the emission was registered (Fig. 1E3,F3,G3) owing to de-aggregation resulting in emission intensities reaching (**TPPOCNHbmC11**) or surpassing (**TPPOCNHbmC2**, **TPPOCNHbmC5**) those in DMF.

*2.2.3. Fluorescence lifetime measurements in DMF and in aqueous solution:* Lifetimes ($\tau$) were obtained from the best fit of the fluorescence decay data with either mono- or bi-exponential functions (Table 1, Fig. B16). In DMF the single species lifetime, $\tau$, obtained is 5 to 20% reduced, compared to that of their parent porphyrins ($\tau$ ~ 11 ns). In PBS, two lifetime values, $\tau 1$ ~1.0 ns and $\tau 2$ ~4.6 ns, were calculated. Each $\tau 1$ and $\tau 2$ species contributes nearly 50% to the total population (entries 1-3). In contrast, in the respective porphyrins (entries 4-6) the % fraction of the $\tau 1$ population increases drastically with linker chain-length whereas the % of the $\tau 2$ populations decreases. These results demonstrate that the conjugates behave similarly, nearly irrespective of the linker chain-length, and are organized into two approximately equal populations of aggregated species, with longer $\tau$2 values and increased % fraction, compared to the parent porphyrins.

**Table 1**

Emission lifetimes ($\tau$) of the porphyrin-βCD conjugates and parent porphyrins alone and with pMβCD, in DMF[i] and in PBS[ii], $\lambda_{exc}$ = 515 nm, 2 μM, 25 ºC.

| *Entry* | *Compound* | *Lifetime (ns) DMF* | *Lifetime (ns) PBS* | | *Lifetime (ns) +pMβCD, PBS* | |
|---|---|---|---|---|---|---|
| | | | *τ1* (%) | *τ2* (%) | *τ1* (%) | *τ2* (%) |
| 1 | **TPPOCNHbmC2** | 9.1 | 1.3 (44.1) | 4.6 (55.9) | 2.6 (5.9) | 14.5 (94.1) |
| 2 | **TPPOCNHbmC5** | 9.9 | 0.8 (47.8) | 4.5 (52.2) | 1.4 (1.9) | 12.6 (98.1) |
| 3 | **TPPOCNHbmC11** | 10.7 | 1.2 (50.4) | 4.8 (49.6) | 1.8 (21.1) | 6.6 (78.9) |
| 4 | **TPPOCOOHC2**[i] | 11.2 | 1.3 (19.4) | 5.3 (80.6) | 12.0 (100) | - |
| 5 | **TPPOCOOHC5**[i] | 10.9 | 0.7 (69.5) | 3.7 (30.5) | 0.7 (7.8) | 11.1 (92.2) |
| 6 | **TPPOCOOHC11**[i] | 11.2 | 0.8 (97.7) | 2.7 (2.3) | 1.0 (94.7) | 5.9 (5.3) |

[i]Panagiotakis et al., 2022, [ii]Phosphate buffer saline containing 4% DMSO (v/v), pH 7.4.

*2.3. Self-assembly into nanoparticles (NPs)*

The above measurements strongly indicate the presence of mostly nanoparticles (NPs) rather than random aggregates in the aqueous solution. To optimize NP formation, solutions of the conjugates were prepared according to "good-bad" methodology (Karikis et al., 2018): **TPPOCNHbmCx** were dissolved in the "good-chaotropic" solvent DMSO and then diluted in the "bad" solvent PBS, reaching a final solution of PBS with 4% DMSO (v/v), pH 7.4 and were allowed to self-assemble at room temperature (r.t.) for 24 h.

*2.3.1 Scanning and Transmission electron microscopies (SEM, TEM)*. The SEM image of the NP assemblies formed by **TPPOCNHbmC11**, initially examined at 100 μM concentration, revealed three predominant populations of round, granular NPs (Fig. B17A1) with average diameters ~500 nm, ~200-300 nm and ~50-100 nm. However, at 20 μM and as TEM images (Fig. 2A and Figs. B17A2, A3) confirm, smaller, rather uniform nanospheres with average diameters of ~70 nm were formed. Few larger particles (~200 - 350 nm, Fig. B17A2) were observed.

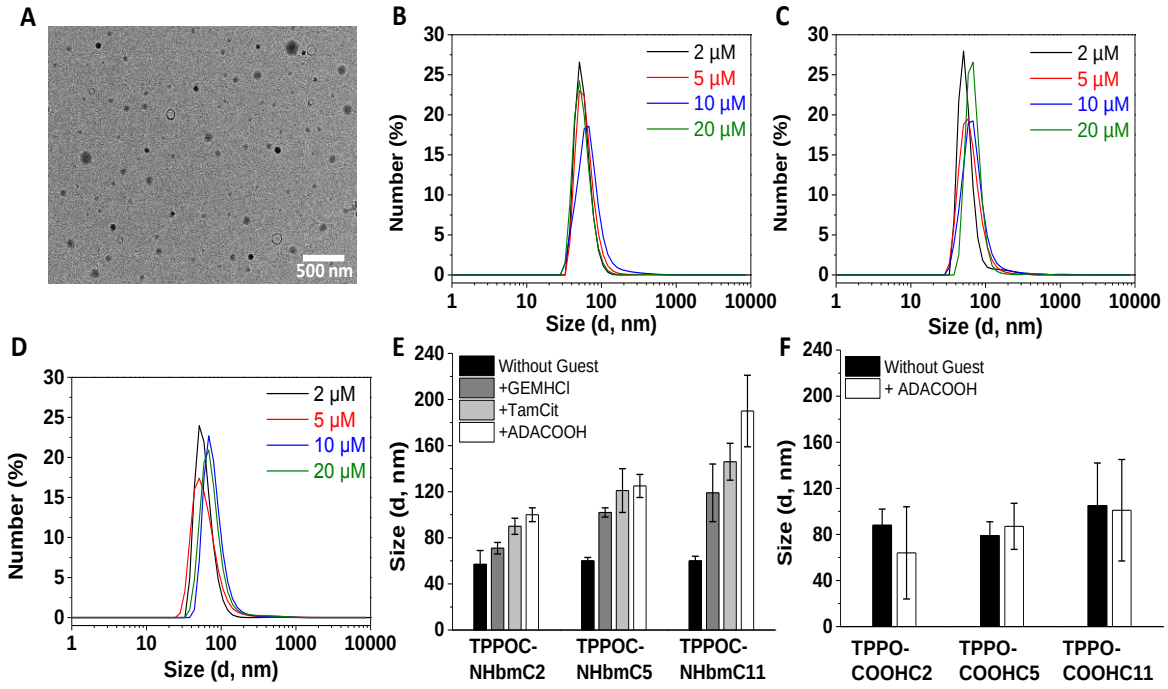


**Fig. 2.** (A) TEM image of **TPPOCNHbmC11** NPs at 20 μM (without contrasting agent); (B-D) Number (%) *vs* size DLS profiles of (B) **TPPOCNHbmC2**, (C) **TPPOCNHbmC5** and (D) **TPPOCNHbmC11** NPs at 2, 5, 10 and 20 μM concentrations in PBS*. DLS profiles of number (%) *vs* size of (E) **TPPOCNHbmCx** in comparison with (F) **TPPOCOOHCx** (2 μM in PBS) and in the presence of guest molecules **(GEM.HCl**, **TamCit**, **ADACOOH**). *PBS is with 4% DMSO (v/v), pH 7.4

Imaging did not require any contrasting agent, suggesting that the NPs may be relatively compact and dense. The EDX experiments (Fig. B17B) confirm the identity of the NPs. The corresponding TEM images of **TPPOCNHbmC5** revealed a rather diffuse material on the grid (data not shown) suggesting that these NPs are more stable in the aqueous solution.

*2.3.2. Dynamic light scattering (DLS).* The pre-assembled conjugates in the range 2 to 20 μM behave uniformly (Fig. 2B-D, Figs. B17C1,C2) and form ~ 60 nm NPs with polydispersity indices (PDI) ≤0.22 (entries 1-3, Table 2), irrespective of the linker between **TPP** and βCD, in contrast to their parent porphyrins (entries 4-6, Table 2). Note that the DLS raw data (% intensity *vs* size) are inevitably affected by the absorption of the porphyrin moieties at the detection wavelength (633 nm) and by the few large NPs that scatter intensely. The conjugates, therefore, seem to share a common self-organization mode. Evidently, the considerable amphiphilic character of the porphyrin-βCD dyad provides π-π stacking domains *via* the strongly hydrophobic **TPP** moieties, while the hydrophilic βCD cups are exposed. The NPs of **TPPOCNHbmC2** and **TPPOCNHbmC5** are stable for 72 h in PBS whereas the NPs of **TPPOCNHbmC11** are stable for 48 h and then increase in size (Fig. B17C3). Among other properties, size affects the entrance, traffic and localization of NPs in cells. NPs of ~50 nm are most suitable for endocytic cell uptake, while NPs of greater dimensions are either less internalized or reside on cell membranes, the mechanisms additionally depending on the surface properties of the NPs (Dolai et al., 2021). Thus, the present NPs seem suitably sized and sufficiently stable for cell experiments.

**Table 2**
DLS measurements of self-assembled conjugates and the corresponding porphyrins, 2 μM in PBS[i] and in the presence of drugs.

| # | Compound[ii] | Size (nm) (PDI[iii]) | | | |
|---|---|---|---|---|---|
| | | **NP** | **+ TamCit[iv]** | **+ GEM[v]** | **+ ADACOOH[vi]** |
| 1 | **TPPOCNHbmC2** | 57 ± 12 (0.22) | 90 ± 7 (0.25) | 71 ± 5 (0.23) | 100 ± 6 (0.23) |
| 2 | **TPPOCNHbmC5** | 60 ± 3 (0.17) | 121 ± 19 (0.24) | 102 ± 4 (0.29) | 125 ± 10 (0.27) |
| 3 | **TPPOCNHbmC11** | 60 ± 4 (0.19) | 146 ± 16 (0.23) | 119 ± 25 (0.23) | 190 ± 31 (0.14) |
| 4 | **TPPOCOOHC2** | 88± 14 (0.39) | - | - | 64± 40 (0.69) |
| 5 | **TPPOCOOHC5** | 79± 12 (0.81) | - | - | 87± 20 (0.91) |
| 6 | **TPPOCOOHC11** | 105± 37 (0.79) | - | - | 101± 44 (0.84) |

[i]Phosphate buffer saline containing 4% DMSO (v/v), pH 7.4, r.t; [ii]Measured 24 h after preparation of the solutions.
[iii]Polydispersity Index; [iv]Tamoxifen (2-[4-[(Z)-1,2-diphenylbut-1-enyl]phenoxy]-*N*,*N*-dimethylethanamine) citrate; [v]Gemcitabine hydrochloride; [vi]1-Adamantyl-anecarboxylic acid.

*2.3.3. Theoretical calculations for self-assembly*. The geometries of the conjugates were optimized using crystallographic coordinates for βCD and porphyrin moieties (Giastas et al, 2003; Charalambidis et al., 2016) at the Molecular Mechanics level of theory using Avogadro software. The calculations showed that due to twisting of the aliphatic linkers near the βCD narrow opening, the maximum molecular dimensions of the optimal geometries of **TPPOCNHbmC5** and **TPPOCNHbmC11** become very similar, ~2.9 nm (Fig. B18), in support of the experimental results.

*2.4. Anticancer drug inclusion in the NPs*

Two, differently structured drugs were considered for loading in the NPs. Tamoxifen (2-[4-[(*Z*)-1,2-diphenylbut-1-enyl]phenoxy]-*N*,*N*-dimethylethanamine) is a selective estrogen receptor modulator drug (SERM) prescribed as citrate salt (**TamCit**) to prevent and treat estrogen receptor positive breast cancer (Osborne, 1998). We have previously determined a substantial 1:1 binding constant (7.0 $\pm 1.5 \times 10^3$ $M^{-1}$) between βCD and *N*-desmethyltamoxifen (**NDTAM**) (Aggelidou et al., 2013) owing to the presence of three phenyl groups in the molecular structure suitable for cavity inclusion. Gemcitabine (**GEM**, 2',2'-difluoro-2'deoxycytidine, dFdC), is a pyrimidine nucleoside analogue anticancer prodrug used in the treatment of a range of solid tumors, also a broad spectrum antiviral agent (Lee et al. 2017) and a potent radiosensitizer (Vanderveken et al., 2016). **GEM** does not carry groups suitable for the cavity of βCD, and binds βCD weakly ($46 \pm 2$ $M^{-1}$), as we derived from NMR titrations (Fig. B19). Since the adamantyl group (**ADA**) is typically considered as an ideally sized moiety for strong βCD inclusion ($10^4$ -$10^5$ $M^{-1}$, Rekharsky & Inoue, 1998), it became clear that the best approach would be to employ a hydrolysable **ADA** derivative of **GEM** in the studies, as needed, and therefore 4-*N*-(1-adamantoyl)-2',2'-difluoro-2'-deoxycytidine (**GEMADA**) was prepared (Scheme A2).

*2.4.1. DLS experiments*. Solutions of the pre-assembled NPs were co-incubated with model guest 1-adamantylcarboxylic acid (**ADACOOH**), **TamCit** and **GEM** (Table 2, Fig. 2E). Incubation with **ADACOOH** results in doubling (**TPPOCNHbmC2/C5**) and tripling (**TPPOCNHbmC11**) of the NP diameters, reaching ~ 200 nm. On the contrary, the aggregates of the parent porphyrins do not seem to be particularly disturbed (Fig. 2F). Consequently, the NPs seem to maintain a number of available cavities and the entering guests push the linker chains away causing the NPs to expand. Incubation with the very poor guest, **GEM**, causes moderate growth of NPs, suggesting that non-cavity entanglement

can be also a loading mechanism. **TamCit** causes the NPs to grow considerably (**TamCit**), exceeding 100 nm for the conjugate with C5 and C11 linkers (Table 2), suggesting both cavity encapsulation and entanglement in the NPs. Table B4 lists $\lambda_{max}$ shfits in the presence of guests. Overall, NPs seem to grow with the length of the chain between βCD and **TPP** moieties, remaining below 200 nm thus still considered suitable for cell studies (Dolai et al., 2021; Oh and Park, 2014). The PDI values remained reasonably low, ranging from 0.14 to 0.29 nm.

*2.4.2 Inclusion studies by NMR.* Direct proof of guest encapsulation in the βCD cavity of **TPPOCNHbmCx** was provided by NMR spectroscopy using pMβCD to cap, isolate and solubilize the **TPP** part. The spectra confirm strong and specific **TPP** moiety inclusion in pMβCD (Fig. B20A-D, Fig. B21). Table B3 lists the stoichiometries and binding constants ($K \sim 10^{11}$ $M^{-2}$, Fig. B22) of pMβCD/conjugate inclusion complexes. The tight pMβCD/**TPPOCNHbmCx** complexes form additional complexes with **TamCit** *via* the available βCD moiety (Fig. B21A, Fig. B21B-D).

*2.4.3 UV-Vis spectral analysis*. Analysis of the absorption spectra in DMF and in PBS of the NPs alone and drug-loaded (Fig. B23) was performed with 2$^{nd}$ derivatives (Fig. B24). In DMF all conjugates display a single sharp peak at the same $\lambda_{max}$ = 418.5 nm (Fig. B24A) confirming the presence of monomers only. In contrast, the conjugates reveal rather broadened and both red- and blue-shifted Soret bands in PBS (Fig. B24B-D): those at ~ 403 nm suggest formation of H-aggregates while the red-shifted ones at ~ 422 nm suggest formation of J-aggregates (Maiti et al., 1998; Villari et al., 2012, Pescitelli et al., 2014). Upon addition of the drugs, the intensities of both bands change suggesting redistribution of the respective populations while bathochromic shifts and further broadening reveal the enhancement of J-aggregates and the enlargement of the NPs, in agreement with the DLS results. Theoretical calculations, as in section 2.3.3, show that entry of **ADACOOH** in the cavity of **TPPOCNHbmC11** untwists the aliphatic chain, resulting in extension of the conjugate from 2.9 nm to 3.6 nm (Fig. B24E).

*2.5. Photostability and $^1O_2$ production*

The decrease in absorption intensity of the Soret bands in the UV-Vis spectra (Fig. B25A-C) was monitored upon irradiation at $\lambda$ = 630 ± 10 nm, 0-28.34 *J*/cm$^2$ corresponding to 0-120 min, in PBS. At ~4 *J*/cm$^2$, used for irradiation of the cells (section 2.8) the photobleaching of all conjugates is only

~ 10% reaching ~30% at the end (Fig. B25D). The similar behavior is attributed to the common assembly mode of NPs in the aqueous medium. Moreover, irradiation of the conjugates in PBS in the presence of 9,10-anthracenediylbis(methylene)dimalonic acid (ABDA) confirmed the generation of $^1O_2$ by all conjugates (Fig. B26), even in as NPs. ABDA is known to react instantly with $^1O_2$ to form an endoperoxide product thus resulting in its photobleaching (Entradas et al., 2020; Song et al., 2017). The rate constants of $^1O_2$ production for **TPPOCNHbmC5**/C**2** (~10 x $10^{-4}$ $M^{-1}$) are similar to or greater than that of the known PS *meso*-5,10,5,20-(3-hydroxyphenyl)porphyrin (**mTHPP**) (~ 6.6 x $10^{-4}$ $M^{-1}$, Table B5) thus indeed, the NPs are photoactive.

*2.6. Confocal Laser Scanning Microscopy*

Live imaging of human breast adenocarcinoma MCF-7 cells incubated for 24 h with NPs of **TPPOCNHbmC5** (Fig. 3A1) and **TPPOCNHbmC2** (Figs. 3A2) using $\lambda_{ex}$ = 514 nm and $\lambda_{em}$ = 637 - 670 nm, revealed abundant and very intense punctate red fluorescence, suggestive of high uptake, in contrast to **TPPOCNHbmC11** (Figs. 3A3, B27) that is not efficiently internalized. The dotted fluorescent patterns observed indicate that the conjugates are localized at numerous intracellular vesicular organelles such as endosomes and lysosomes. There are no indications of either cytoplasm or nuclear membrane localization. Brief co-incubation of the **TPPOCNHbmC2**-treated cells with LysoTracker® Green DND-26 ($\lambda_{ex}$ = 488 nm, $\lambda_{em}$ = 501 - 538 nm) resulted in multiple yellow dotted areas in the overlaid images (Figs. 3B1-B3, B28), supporting localization of the conjugates in the lysosomes. Mander's Coefficients (M1 and M2) (Manders et al., 1993; Pike et al., 2017) were calculated and M1 (fraction of red fluorescence, i.e. **TPPOCNHbmC2** in areas with green fluorescence, i.e. LysoTracker) was found >0.80 (Fig. B28E) proving the exceptional selectivity of **TPPOCNHbmC2** NPs in targeting the lysosomes.

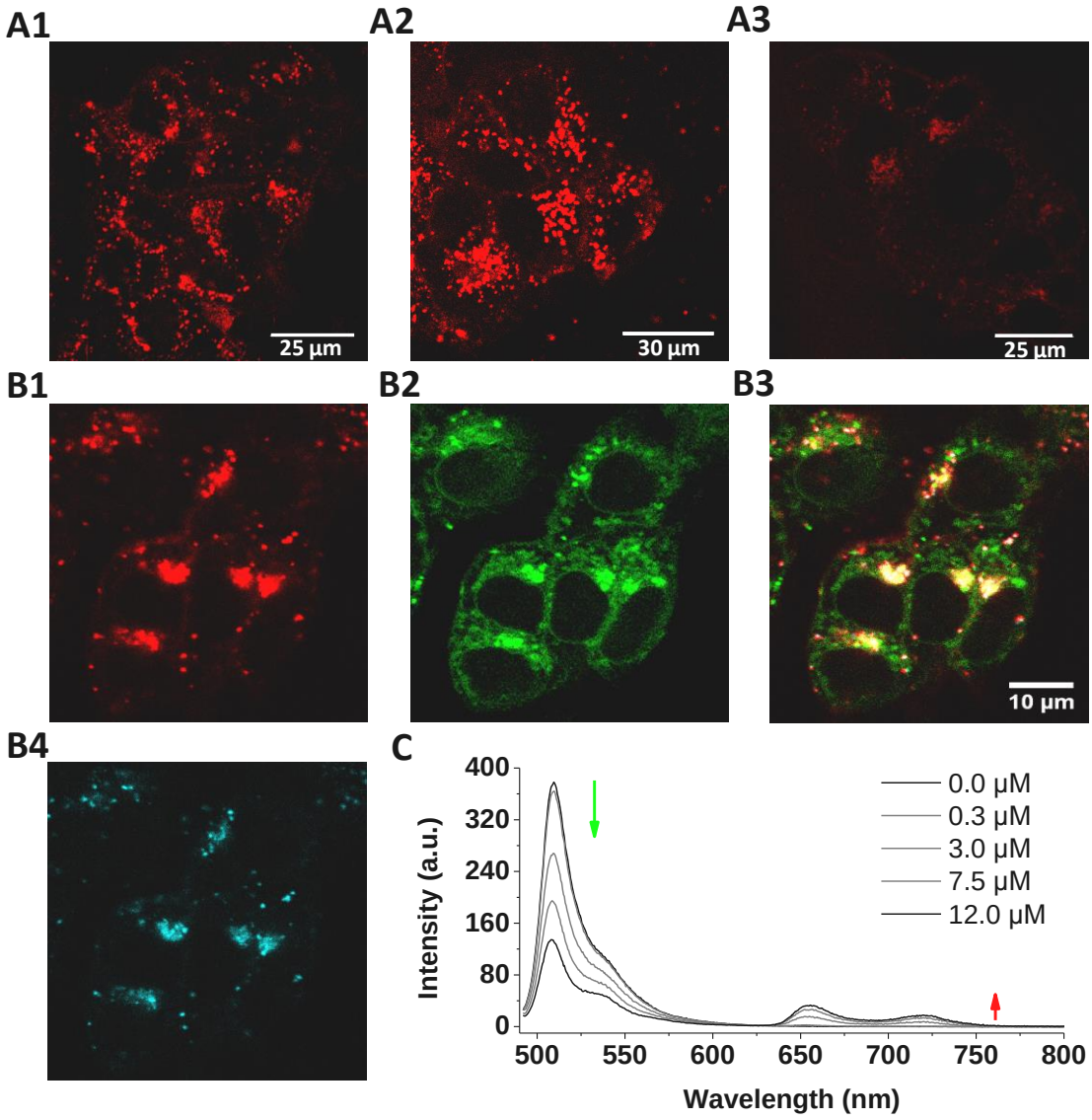


**Fig. 3. (**A-B): Confocal microscopy images of MCF-7 cells incubated for 24 h with NPs of conjugates (10 µM): (A1-3, B1) images with $\lambda_{ex}$ = 514 nm, laser intensity 3% and $\lambda_{em}$ = 637 - 670 nm: (A1) **TPPOCNHbmC2**; (A2) **TPPOCNHbmC5**; (A3) **TPPOCNHbmC11**; B1) **TPPOCNHbmC2** NPs treated with LysoTracker® Green DND-26 (0.3 µM); (B2) cells of B1 imaged with $\lambda_{ex}$ = 488 nm, laser intensity 1%, $\lambda_{em}$ = 501 - 538 nm; (B3) overlay of images B1 and B2 with yellow spotted areas indicating high co-localization; (B4) cells in B1 imaged with $\lambda_{ex}$ = 488 nm and laser intensity 3% but detected with $\lambda_{em}$ = 637 - 670 nm indicates FRET between the lysotracker and the porphyrin moiety of **TPPOCNHbmC2**; (C) Decreased emission at $\lambda_{em}$ = 510 nm (green arrow) of a LysoTracker® Green DND-26 solution (0.3 µM) in the presence of increased amounts of **TPPOCNHbmC2** (0-12 µM) and emergence of **TPPOCNHbmC2** fluorescence at $\lambda_{em}$ = 625 - 760 nm (red arrow) registered following $\lambda_{exc}$ = 488 nm in PBS* indicate FRET between the two molecules.. * PBS is with 4% DMSO (v/v), pH 7.4.

Interestingly, examination of the cells incubated with **TPPOCNHbmC2** (Fig. 3B1,B2) with $\lambda_{ex}$ = 488 nm but $\lambda_{em}$ = 637 - 670 nm, resulted in an image (Fig. 3B4) identical to that of Fig. 3B1. In

parallel, cells incubated only with LysoTracker and imaged with $\lambda_{ex}$ = 514 nm did not reveal red fluorescence at $\lambda_{em}$ = 637 - 670 nm (Fig. B29A1-A3). Moreover, cells incubated with **TPPOCNHbmC2** alone but imaged with $\lambda_{ex}$ = 488 nm did not reveal any fluorescence at $\lambda_{em}$ = 637 - 670 nm (Fig. B29B1-B3). The above indicate that the image in Fig. 3B4 has resulted from an in-cell Förster resonance energy transfer (FRET) effect between the lysotracker (donor) and **TPPOCNHbmC2** (acceptor), thus the respective molecules are in very close proximity (<10 nm). Further confirmation of FRET was obtained in solution: upon addition of **TPPOCNHbmC2** gradual quenching of the lysotracker emission band at 510 nm solution was registered**,** either using $\lambda_{ex}$ = 488 (Fig. 3C) or 470 nm (Fig. B29C). Concomitant increase of the bands at 654 and 716 nm due to the emission of the porphyrin moiety was noted. The rate of quenching was nearly identical at both $\lambda_{ex}$ settings (Fig. B29D) and there was no **TPPOCNHbmC2** emission (Fig. B29E). The LysoTracker used is a BODIPY derivative that when in lysosomes, can presumably enter available βCD cavities of co-localized conjugates keeping the chromophores at FRET distance. Similar effects have been recently reported in cells between a BODIPY-pMβCD conjugate (donor) and an included porphyrin (acceptor) (Nakagami et al., 2021).

The self-assembled NPs are apparently taken up by the cells *via* endocytosis thus they end up in vesicles within the cells. The very bright fluorescence intensity in the images suggests that it is possible to find monomeric conjugates anchored in the organelle membranes, thus model liposomes were employed as mimics of subcellular compartments to investigate such a possibility.

*2.7. Liposomes as models of vesicular organelles- incorporation of the conjugates in the membranes*

1,2-Dioleoyl-*sn*-glycero-3-phosphocholine (DOPC) liposomes were prepared by the Bangham method (Bangham et al., 1965) in the presence of **TPPOCNHbmC5** ,**TPPOCNHbmC11** or **TPP**. The incorporation efficiency of the conjugates was very high (> 99%). The size, size distribution, zeta potential, and morphology of the resulting liposomes were indicative of stable and well-formed entities (Table B6, Fig. B30). Comparison of the UV-Vis absorption of the DOPC/conjugates liposomes in water with those of the respective conjugates in DMF (Fig. B31), where the conjugates are presumably monomeric, reveals complete similarity regarding both $\lambda_{max}$ and band shape. This remarkable result suggests that the conjugates have been incorporated in the liposome membranes as monomers and the absorption bands do not arise from NPs enclosed in the liposome aqueous interior, where they are expected to aggregate and give rise to much broadened bands. Additionally,

overnight co-incubation of blank DOPC liposomes with a 2 μM PBS solution of pre-assembled porphyrin-βCD NPs resulted in increased absorption intensity and decreased broadness of the Soret band for **TPPOCNHbmC2/C5** NPs (Figs. B32A,B,D), suggestive of their effective interaction with the liposome membranes. In contrast, **TPPOCNHbmC11** displayed slightly greater broadness of the Soret band (Fig. B32C) probably due to the prevailing enlargement of the NP size with time (Fig. B17C3).

Using a liposome irradiation setup (~50 mW/cm², 300-400 nm centered at 350 nm) the successful production of ROS by **TPPOCNHbmC5** in DMF was confirmed using the ROS scavenger methyl linoleate, (Fig. B33). The DOPC/**TPP**/CF liposomes loaded with carboxyfluorescein (CF) as model cargo showed clear release of CF with irradiation time (Fig. B34A), demonstrating that the integrity of the liposome membrane has been compromised due to the ROS generated by **TPP**. Surprisingly, the release profile of CF from the formulation DOPC/**TPPOCNHbmC5**/CF (Fig. B34B) was practically that of the blank liposomes loaded with CF. Excitation of a CF solution in PBS at $\lambda_{exc}$ = 470 nm (Massu et al., 2000) and gradual increase the amounts of **TPPOCNHbmC5** added (no absorption at 470 nm) revealed decreased CF emission (Fig. B34C). The emission spectrum of CF ($\lambda_{em}$ = 480 - 600 nm), overlaps with the absorption region of **TPPOCNHbmC5** (350 - 680 nm, Fig. 1) and FRET between the CF donor and the porphyrin moiety acceptor in **TPPOCNHbmC5** mediated by the βCD cavity can result in decreased CF emission and emergence of **TPPOCNHbmC5** fluorescence (653 and 715 nm, Fig. B34C). Indeed, the 2D ROESY NMR spectrum of βCD/CF confirmed very strong binding (Fig. B34D) undisturbed by the addition of the competitive guest **ADACOOH**.

The liposome experiments show that the conjugates, even as assembled NPs, can be incorporated in the bilayers as monomers. Moreover, guest release from the interior of the liposomes can be greatly affected by the formation of strong inclusion complexes with available βCD cavities. The in-cell FRET between **TPPOCNHbmC2** and LysoTracker described previously (Fig. 3) suggests that by analogy, molecules entrapped in the lysosomes can also form inclusion complexes with the available cavities of the membrane-embedded conjugates.

*2. 8. Cytotoxicity and photokilling – a synergistic PCI effect*

MCF-7 cells were incubated in 96-well plates for 24 h with either the pre-assembled NPs alone or with the drug-loaded NPs (with **TamCit** and **GEMADA**) or with the drugs alone. The appropriate

sample groups were then irradiated at 640 nm with a custom-made LED array lamp at light-doses suitable to achieve $LD_{50}$ or the highest synergistic effect (4.18 *J*/cm$^2$, Figs. B35A-C). Irradiation of the untreated cells confirmed that light alone does not induce toxicity (Fig. B35D). Subsequently, all plates including dark, media only, and drug only controls, were evaluated for cytotoxicity with the MTT assay at the 24 h and 48 h time-points (Fig. 4).

The dark experiments of Fig. 4A reveal that **TamCit** and **GEMADA** alone confer low toxicity on the cells at 24 h (< 20% cell death), compared to dark control, and have similar effects after 48 h. The conjugates alone at the selected concentrations (Figs. 4B-D) are devoid of toxicity in the dark at 24 h and the cells seem to recover with time (48 h). Similarly, the cells with the NPs loaded with either **TamCit** or **GEMADA** largely retain their viability at 24 h and even proliferate at 48 h, demonstrating lack of dark toxicity, despite the chemotoxic payload (Fig. 4B-D).

Upon irradiation, the drugs alone at 24 h and 48 h (Fig. 4A) confer little damage, and the viability of the cells is retained at ~80% with a tendency to recover with time. On the contrary, the conjugates **TPPOCNHbmC2** (Fig. 4B) and **TPPOCNHbmC5** (Fig. 4C) elicit considerable toxicity as only ~30% of the cells remain viable at 24 h, displaying strong phototoxic (PDT) effects. Nevertheless, the cells proliferate after additional 24 h (~60 % viability) indicating that at the given set of experimental conditions the phototoxicity effect is temporary. In sharp contrast, the **TPPOCNHbmC2** and **TPPOCNHbmC5** NPs loaded with either **TamCit** or **GEMADA** not only confer stronger PDT effects on the cells at 24 h (~15-20% viability) but they also halt the proliferation of the cells for the next 24 h suggesting action of the drugs and manifestation of PCI. Under the same conditions, cells incubated with **TPPOCNHbmC11** NPs alone or loaded with the drugs, show poor PDT effects (~70% viability at 24 h) and questionable PCI effects (Fig. 4D), evidently due to low uptake (Fig. 3A3). The unloaded conjugates' phototoxicity compares sufficient well with that of **mTHPP** used as a positive control (Fig. B36) which, however, has very different localization preferences in the cells. Different localization locci had also been observed in our previously reported water soluble conjugates (Aggelidou et al. 1013), which were also less efficient regarding PDT than the current, insoluble amphiphilic systems.

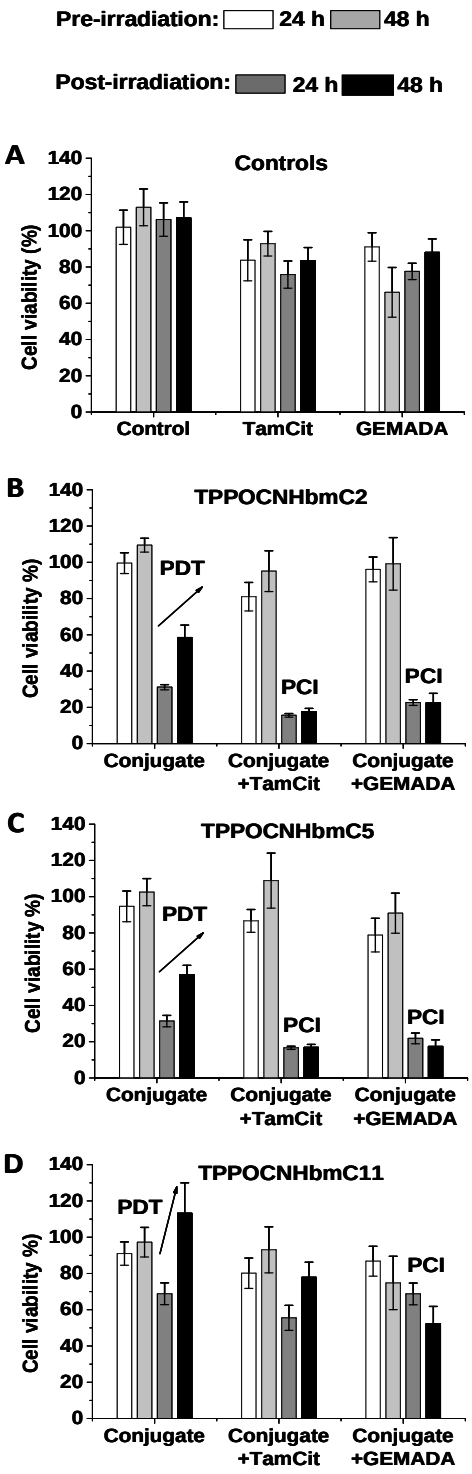


**Fig. 4.** Viability of MCF-7 cells following 24 h incubation with porphyrin-βCD NPs (10 μM) without or with anticancer drugs (7.5 μM), without (white and light grey bars) or with irradiation at 4.18 $J/cm^2$, $\lambda$ = 640 nm (dark grey and black bars). The MTT assays were performed at 24h (dark grey bars) or 48 h (black bars) post-irradiation: (A) Control experiments with cells alone (control), **TamCit** or **GEMADA**; (B) **TPPOCNHbmC2**; (C) **TPPOCNHbmC5**; (D) **TPPOCNHbmC11**, alone and loaded with the drugs. Error bars are shown in each case.

The results with the drug-loaded **TPPOCNHbmC2/C5** NPs show strong synergy between the photodynamic and chemotherapeutic effects (Table B7): the values of the calculated synergy index, $\alpha$, (Christie et al., 2016, Appendix A) are ~1.5 at 24 h and ~3 at 48 h. This outcome can be convincingly explained by $^1O_2$ photogeneration that compromises lysosome membranes and subsequently induces drug release (PCI). Strong synergy is observed not only with **TamCit**, a drug suitable for treatment of the estrogen-receptor β-positive MCF-7 cell line, but also with **GEMADA**. The first line anticancer drug **GEM** requires nucleoside transporters for cell uptake (Mackey et al., 1999). When intracellularly, **GEM** undergoes sequential phosphorylation steps to attain the active form that inhibits both DNA synthesis and the enzymes of nucleotide metabolism of cancer cells (Baker et al., 1991; Mini et al., 2006). In our comparison experiments, the cell viability using **GEM** alone is found to decrease to ~60% after either 24 h or 48 h incubation, with or without irradiation (Fig. B37) suggesting low uptake. **GEMADA** alone, under the same conditions, appears to be even less toxic than **GEM** (Fig. B36) as cell viability only drops to ~80%. On the contrary, under irradiation conditions, the cells treated with **GEMADA**-loaded NPs suffer profound reduction of their viability (Figs. 4B-C), as discussed above. We can postulate, therefore, that due to the presence of the adamantyl group **GEMADA** binds strongly with the βCD cavities of the NPs and is endocytosed along with them, thus bypassing considerably its difficulty for uptake and potentially minimizing off-target effects. Under irradiation the drug is released to exert its toxic effects on-site. Various **GEM** modifications to overcome current drawbacks and improve its clinical efficacy have been reported (Moysan, et. al., 2013). Here, the adamantyl group is bonded to the 4-(*N*)- position of **GEM** (Scheme A2) leaving the –OH site free for phosphorylation and possibly also protecting the molecule against immediate deamination by cytidine deaminase, a process considered responsible for resistance to the drug. Our approach to **GEM** modification may prove suitable for other drugs of the nucleoside analogue family for delivery *via* similar nano-platforms.

The aggregating properties of glycosylated or "sugar-coated" porphyrinoids have been recognized, investigated and assessed and their importance in the diagnostic and therapeutic outcome has been highlighted (Singh et al, 2015). Many parameters contribute to the size and stability of the aggregates that affect both the photophysical properties and cell uptake. The results presented herein demonstrate that uncomplicated porphyrin-βCD conjugates form suitable NPs and that loading with small molecular weight chemotherapeutic drugs or tailored pro-drugs, is feasible.

Interaction with cell membrane components is expected to destabilize the NPs, however, it is also expected that even <60 nm entities would be large enough (MW ~2 kDa) to become endocytosed and end up in endosomes and lysosomes. Further, the fact that upon irradiation **GEM** alone confers little damage to the cells and **GEMADA** alone even less, but the **GEMADA**/conjugate formulation becomes highly toxic, highlights a method to bypass natural cell uptake mechanisms and direct the drug together with the conjugate into the lysosomes for PCI. Our present NPs, completely devoid of dark toxicity, can be enlisted as a promising new set of biocompatible systems and can be considered, in addition to other nano-assemblies (Xue et al, 2019), as efficient vehicles for the photodelivery of small drugs.

## 3. Conclusions

In a few synthetic steps we have prepared three conjugates of βCD with monocarboxy-methyl-, -butyl and -decyl-**TPP**. The conjugates show similar photophysical properties both in DMF and in aqueous media, regardless of the different length of the aliphatic chain linkers between the **TPP** and βCD moieties. Importantly, the conjugates self-assemble into very similarly sized, photoactive NPs that specifically target and accumulate in the lysosomes of MCF-7 cells. Liposome experiments show that the NPs can interact with lipid membranes wherein they can be lodged as monomers. We demonstrate high overall photo and chemo-toxicities following irradiation of cells incubated with NPs loaded with **TamCit** or **GEMADA** due to significant synergy developed that suggests operation of PCI, the effects lasting for at least 48 h. Dark experiments demonstrate complete lack of toxicity of the NPs, either empty or drug-loaded, thus the drugs are released only with the action of light. Moreover, attachment of an adamantyl group can direct **GEM** along with the NPs to endocytic vesicles, enabling use of this potent small drug in PCI treatments. The radiosensitizing properties of **GEM** also point to the possibility that the NPs could be interesting vehicles for combined chemo-, photo- and radio- treatment of tumors.

## CRediT authorship contribution statement

S.P.: Investigation, Methodology, Analysis, Writing & Editing; B.M. and A.A.: Methodology, Analysis & Editing; L. B.-M. Investigation, Analysis, & Writing; T.R.: Methodology & Analysis; A.R.R.: Investigation & Analysis; N.B.: Methodology & Review; G. C.: Methodology & Editing;

A.G.C. Resources & Review; M. G.: Methodology, Analysis; T.A.T.: Resources, Analysis, Review; K. B.: Resources, Analysis & Review; C. L.: Resources, Analysis, Review; M. P.: Resources, Analysis, Review; K.Y.: Conceptualisation, Investigation, Analysis, Writing, Review and Editing, Acquisition of funds, Resources, Coordination.

**Declaration of competing interest**

There are no conflicts to declare.

*Acknowledgments*

*Funding*

Funding by the General Secretariat for Research and Technology (Greece) in the frame of the EuronanoMed II network for the project PCInano (T3EPA-0048) and infrastructure support by the project "National Infrastructure in Nanotechnology, Advanced Materials and Micro-/ Nanoelectronics" INNOVATION EL (MIS 5002772) funded by the Operational Programme "Competitiveness, Entrepreneurship and Innovation" (NSRF 2014-2020) and co-financed by Greece and the European Union are gratefully acknowledged.

**Appendix A and Appendix B. Experimental and Supplementary data**

## References


Aggelidou, C., Theodossiou, T. A. & Yannakopoulou, K. (2013) Protoporphyrin IX-β-cyclodextrin bimodal conjugate: nanosized drug transporter and potent phototoxin, *Photochem. Photobiol*., 89, 1011-1019. doi: 10.1111/php.12127

Agostinis, P., Berg, K., Cengel, K. A.; Foster, T. H., Girotti, A. W., Gollnick, S. O.; Hahn, S. M., Hamblin, M. R., Juzeniene, A., Kessel, D.; Korbelik, M., Moan, J.; Mroz, P., Nowis, D., Piette, J., Wilson, B. C. & Golab, J. (2011). Photodynamic therapy of cancer: an update. *CA-Cancer J. Clin.*, *61*, 250−281. doi:10.3322/caac.20114.

Baker, C. H, Banzon, J., Bollinger, J. M., Stubbe, J., Samano, V., Robins, M. J., Lippert, B., Jarvi, E. & Resvick, R. (1991). 2'-Deoxy-2'-methylenecytidine and 2'-deoxy-2',2'-difluorocytidine 5'-diphosphates: potent mechanism-based inhibitors of ribonucleotide reductase. *J. Med. Chem.*, *34(6)*, 1879-1884. doi: 10.1021/jm00110a019

Bangham, A. D., Standish, M. M. & Watkins, J. C. (1965). Diffusion of univalent ions across the lamellae of swollen phospholipids. *J. Molecular Biol.*, *13(1)*, 238-252. doi.org/10.1016/S0022-2836(65)80093-6

Charalambidis, G., Georgilis, E., Panda, M., K., Anson, C. E, Powell, A. K., Doyle, S., Moss, D., Jochum, T., Horton, P. N., Coles, S. J, Linares, M., Blejonne, D., Naubron, J-V., Conradt, J., Kalt, H., Mitraki, A., Coutsolelos, A. G. & Balaban, T. S.. (2016). A switchable self-assembling and disassembling chiral system based on a porphyrin-substituted phenylalanine–phenylalanine motif. *Nature Comm*., *7*, 12657. doi: 10.1038/ncomms12657

Christie, C., Molina, S., Gonzales, J., Berg, K., Nair, R. K., Huynh, K., Madsen, S. J. & Hirschberg, H. (2016). Synergistic chemotherapy by combined moderate hyperthermia and photochemical internalization. *Biomedical Optics Express*, *7(4)*, 1240-1250. doi:10.1364/BOE.7.001240

Dabrowski, J. M., Pucelik, B., Regiel-Futyra, A., Brindell, M., Mazuryk, O., Kyzioł, A., Stochel, G., Macyk, W. & Arnaut, L.G. (2016). Engineering of relevant photodynamic processes through structural modifications of metallotetrapyrrolic photosensitizers. *Coord. Chem. Rev.*, *325*, 67–101. doi.org/10.1016/j.ccr.2016.06.007.

Dolai, J., Mandal, K. & Jana, N. R. (2021). Nanoparticle size effects in biomedical applications, *ACS Appl. Nano Mater*., 4, 7, 6471–6496. doi.org/10.1021/acsanm.1c00987

Dolmans, D. E. J. G. J., Fukumura, D. & Jain, R. K. (2003). Photodynamic therapy for cancer. *Nat. Rev. Cancer*, *3*, 380−387. doi: 10.1038/nrc1071.

Entradas, T., Waldron, S. & Volk, M. (2020). The detection sensitivity of commonly used singlet oxygen probes in aqueous environments. *J. Photochem. Photobiol, B Biology*, 204, 111787. doi.org/10.1016/j.jphotobiol.2020.111787

Fraix, A., Goncalves, A. R., Cardile, V., Graziano, A. C. E., Theodossiou, T. A., Yannakopoulou,K. & Sortino, S. (2013). A multifunctional bichromophoric nanoaggregate for fluorescence imaging and simultaneous photogeneration of RNOS and ROS. *Chem Asian J.*, *8*, 2634 – 2641. doi: 10.1002/asia.201300463

Giastas, P., Yannakopoulou, K. & Mavridis, I. M. (2003). Molecular structures of the inclusion complexes β-cyclodextrin/1,2-bis(4-aminophenyl)ethane and β-cyclodextrin/4,4´-diaminobiphenyl. Packing of dimeric β-cyclodextrin inclusion complexes, *Acta Crystallogr*., *B59*, 287-299. doi: 10.1107/S010876810300257X

Jerjes, W., Theodossiou, T. A., Hirschberg, H., Høgset, A., Weyergang, A., Selbo, P. K., Hamdoon, Z, Hopper, C. & Berg, K. (2020). Photochemical internalization for intracellular drug delivery. From basic echanisms to clinical research *J. Clin. Med.*, *9*, 528. doi: 10.3390/jcm9020528.

Karikis, K.; Butkiewicz, A.; Folias, F.; Charalambidis, G.; Kokotidou, C.; Charisiadis, A.; Nikolaou, V.; Nikoloudakis, E.; Frelek, J.; Mitraki, A.; Coutsolelos, A. G. (2018). Self-assembly of (boron-dipyrromethane)- diphenylalanine conjugates forming chiral supramolecular materials. *Nanoscale*, *10*, 1735. DOI: 10.1039/c7nr08667a

Kessel, D., Obaid, G. & Rizvi, I. (2022). Critical PDT theory II: Current concepts and indications. *Photodiagnosis and Photodynamic Therapy*, *39*, 102923. doi.org/10.1016/j.pdpdt.2022.102923

Kunishima, M., Kawachi, C., Monta, J., Terao, K., Iwasaki, F., Tani, S. (1999). 4-(4,6-Dimethoxy-1,3,5-triazin-2-yl)-4-methyl-morpholinium chloride: an efficient condensing agent leading to the formation of amides and esters. *Tetrahedron, 55(46)*, 13159–13170. doi:10.1016/s0040-4020(99)00809-1

Lee, K., Kim, D.-E., Jang, K.-S., Kim, S.-J., Cho, S. & Kim, C. (2017). Gemcitabine, a broad-spectrum antiviral drug, suppresses enterovirus infections through innate immunity induced by the inhibition of pyrimidine biosynthesis and nucleotide depletion, *Oncotarget*, 8(70), 115315-115325. doi: 10.18632/oncotarget.23258.

Mackey, J. R. , Yao, S. Y., Smith, K. M., Karpinski, E., Baldwin, S. A. ,Cass, C. E., & Young, J. D. (1999). Gemcitabine transport in xenopus oocytes expressing recombinant plasma membrane mammalian nucleoside transporters. *J. Natl. Cancer Inst,. 91*, 1876–1881 doi: 10.1093/jnci/91.21.1876

Maiti, N. C., Shyamalava Mazumdar & N. Periasamy (1998). J- and H-aggregates of porphyrin-surfactant complexes: time-resolved fluorescence and other spectroscopic studies, *J. Phys. Chem. B, 102*, 1528-1538. doi.org/10.1021/jp9723372.

Mandal, A. K., Taniguchi, M., James R. Diers, J. R., Niedzwiedzki, D. M., Kirmaier, C., Lindsey, J. S., Bocian, D. F. & Holten, D. (2016). Photophysical properties and electronic structure of porphyrins bearing zero to four *meso*-phenyl substituents: new insights into seemingly well understood tetrapyrroles. *J. Phys. Chem.*, *120*, 9719-9731. doi: 10.1021/acs.jpca.6b09483

Manders, E. M. M., Verbeek, F. J. & Aten, J. A. (1993). Measurement of co-localization of objects in dual-colour confocal images. *J. Microscopy*, *169(3)*, 375-382. doi.org/10.1111/j.1365-2818.1993.tb03313.x.

Massou, S., Albigot, R. & Prats, M. (2000). Carboxyfluorescein fluorescence experiments. *Biochemical Education*, 28(3), 171-173. doi.org/10.1016/S0307-4412(00)00002-9

Mavridis, I. M & Yannakopoulou, K. (2020). Porphyrinoid−cyclodextrin assemblies in biomedical research: an update, *J. Med. Chem.*, 63, 3391−3424, doi:10.1021/acs.jmedchem.9b01069

Mini, E., Nobili, S., Caciagli, B., Landini, I.& Mazzei, T. (2006). Cellular pharmacology of gemcitabine. *Annals Oncol. 17 (Supplement 5): v7–v12.* doi:10.1093/annonc/mdj941

Moysan, E., Bastiat, G., Benoit & J.-P. (2013). Gemcitabine versus modified gemcitabine: a review of several promising chemical modifications, *Mol. Pharmaceutics, 10*, 430−444. doi.org/10.1021/mp300370t

Nakagami, A., Mao,Q., Gouhier,G., Arima,H. & Kitagishi, H. (2021). FRET-based in-cell detection of highly selective supramolecular complexes of *meso* tetraarylporphyrin with peptide/BODIPY-modified per-*O*-methyl-β-cyclodextrins. *ChemBioChem*, *22*, 1-10. doi: 10.1002/cbic.202100380

Oh, N. & Park, J.-H. (2014). Endocytosis and exocytosis of nanoparticles in mammalian cells. *Int. J. Nanomed*. 9 (Suppl 1) 51–63. doi.org/10.2147/IJN.S26592

Ormond, A. B. & Freeman, H. S. (2013). Effects of substituents on the photophysical properties of symmetrical porphyrins. *Dyes and Pigments, 96*, 440-448. doi.org/10.1016/j.dyepig.2012.09.011

Osborne, C. K. *New Engl. J. Med.* 1998, 339, 1609 -1618. doi: 10.1056/NEJM199811263392207; https://www.cancer.gov/publications/dictionaries/cancer-drug/def/tamoxifen-citrate.

Pike, J. A., Styles, I. B., Rappoport J. Z.& Heath, J. K. (2017).Quantifying receptor trafficking and colocalization with confocal microscopy. *Methods*, *115*, 42-54. doi.org/10.1016/j.ymeth.2017.01.005

Panagiotakis, S., Mavroidi, B., Athanasopoulos, A., Charalambidis, G., Coutsolelos, A. G., Paravatou-Petsotas, M., Pelecanou, M., Mavridis, I. M. & Yannakopoulou, K. (2022). Unsymmetrical, monocarboxyalkyl *meso*-arylporphyrins in the photokilling of breast cancer cells using permethyl-β-cyclodextrin as sequestrant and cell uptake modulator. *Carbohydr. Polymers., 75*, 118666. doi: 10.1016/j.carbpol.2021.118666

Petter, R. C., Salek, J. J., Sikorski, C. T., Kumaravel, G. & Lin, F.-T. (1990). Cooperative binding by aggregated mono-6-(alkylamino)-beta-cyclodextrins. *J. Am. Chem. Soc*., *112*, 10, 3860–3868. doi.org/10.1021/ja00166a021

Pescitelli, G., Di Bari, L. and Berova, N. (2014). Application of electronic circular dichroism in the study of supramolecular systems. *Chem. Soc. Rev*., *43*, 5211-5233. doi: 10.1039/c4cs00104d

Rekharsky, M. V. & Inoue, Y. (1998). Complexation thermodynamics of cyclodextrins. *Chem. Rev*. *98(5)*, 1875-1918. doi: 10.1021/cr970015o

Saokham, P., Muankaew, C., Jansook, P.3, & Loftsson, T. (2018). Solubility of cyclodextrins and drug/cyclodextrin complexes. *Molecules*, *23*, 1161. doi:10.3390/molecules23051161.

Shi, Y. Zhang, F. & Linhardt R. J. Porphyrin-based compounds and their applications in materials and medicine. (2021). *Dyes and Pigments*, 188, 1091362021. doi.org/10.1016/j.dyepig.2021.109136

Singh, S., Aggarwal, A., Bhupathiraju, N. V. S. D. K., Arriana, G., Tiwari K. & Drain, C. M. (2015). Glycosylated porphyrins, phthalocyanines, and other porphyrinoids for diagnostics and therapeutics, *Chem. Rev*. 115, 18, 10261–10306. doi: 10.1021/acs.chemrev.5b00244

Song, R., Feng, Y., Wang, D., Xu, Z., Li, Z. & Shao, X. (2017). Phytoalexin phenalenone derivatives inactivate mosquito larvae and root-knot nematode as type-II photosensitizer. *Sci*. *Rep*. 7, 42058. doi: 10.1038/srep42058

Sultan, A.A., Jerjes, W., Berg, K. , Høgset, A., Mosse, C. A., Hamoudi, R., Hamdoon, Z., Simeon, C., Carnell, D., Forster, M. & Hopper, C. (2016). Disulfonated tetraphenyl chlorin (TPCS2a)-induced photochemical internalisation of bleomycin in patients with solid malignancies: a phase 1, dose-escalation, first-in-man trial. *Lancet Oncol*. *16*, 1217-1229. DOI.org/10.1016/S1470-2045(16)30224-8

Theodossiou, T. A. Goncalves, A. R., Yannakopoulou, K., Skarpen, E. & Berg, K. (2015). Photochemical internalization of tamoxifens transported by a "Trojan-Horse" nanoconjugate into breast-cancer cell lines. *Angew. Chem. Int. Ed*., *54(16)*, 4885–4889. : 10.1002/anie.201500183.

Vanderveken, O. M. Szturz, P., Specenier, P., Merlano, M., Benasso, M., Van Gestel, D., Wouters, K., Van Laer, C., Van Den Weyngaert, D., Peeters, M. & Vermorken, J. B. (2016). Gemcitabine-based chemoradiation in the treatment of locally advanced head and neck cancer: systematic review of literature and meta-analysis. *The Oncologist*, 21, 57-91. doi.org/10.1634/theoncologist.2015-0246

Villari, V., Mineo, P., Scamporrino, E., Micali, N. (2012). Spontaneous self-assembly of water-soluble porphyrins having poly(ethylene glycol) as branches: dependence of aggregate properties from the building block architecture, *Chem. Phys.*, *409*, 23–31. doi.org/10.1016/j.chemphys.2012.09.022

Xue, X., Lindstrom, A. &Li, Y. (2019). Porphyrin-based nanomedicines for cancer treatment, *Bioconjugate Chem*. 30, 6, 1585–1603. doi.org/10.1021/acs.bioconjchem.9b00231

Zhang, C.-W., Zhang, J.-G., Yang, X., Du, W.-L., Yu, Z.-L., Lv, Z.-Y. & Mou, X.-Z. (2022). Carbohydrates based stimulus responsive nanocarriers for cancer-targeted chemotherapy: a review of current practices. *Expert Opinion on Drug Delivery*, *19(6)*, 623-640. doi: 10.1080/17425247.2022.2081320